PROCEEDINGS OF SCIENCE

Gravitational waves from cosmological first-order phase transitions with self-consistent hydrodynamics

Xiao Wang,[a] **Chi Tian**[b] **and Csaba Balazs**[a,*]

[a] *School of Physics and Astronomy, Monash University*
Melbourne, Victoria 3800, Australia

[b] *School of Physics and Optoelectronics Engineering, Anhui University*
Hefei, Anhui 230601, China

E-mail: xiao.wang1@monash.edu, ctian@ahu.edu.cn, csaba.balazs@monash.edu

Gravitational waves (GWs) from first-order cosmological phase transitions (FOPTs) provide a unique window into fundamental physics beyond the Standard Model. This article outlines recent advancements in self-consistent hydrodynamic simulations for predicting GW spectra from FOPTs. By deriving the equation of state directly from the effective potential and resolving the bubble wall velocity and plasma hydrodynamics, our approach enables precise predictions that rely on the effective potential of the input particle physics model. We demonstrate the methodology using the $|\mathrm{H}|^6$ extension of the Standard Model, comparing results with conventional approaches, and highlight implications for future space-based GW observatories such as LISA, DECIGO, and BBO.

Proceedings of the Corfu Summer Institute 2024 "School and Workshops on Elementary Particle Physics and Gravity" (CORFU2024) 12 - 26 May, and 25 August - 27 September, 2024
Corfu, Greece

*Speaker

ISSN 1824-8039. Published by SISSA Medialab.

https://pos.sissa.it/

PoS(CORFU2024)261

1. Introduction

A decade after LIGO/Virgo's first gravitational wave (GW) detection [1], we stand on the verge of observing the stochastic gravitational wave background (SGWB). Recent Pulsar Timing Array results hint at this milestone [2–5]. Cosmological first-order phase transitions (FOPTs) are a key SGWB source which, at the electroweak scale, produce GWs detectable by space-based experiments such as LISA, TianQin, and DECIGO [6–8]. FOPTs also probe beyond-the-Standard-Model (BSM) physics, making phase transition gravitational waves (PTGWs) a novel tool for discovery.

Quantifying PTGWs requires understanding their production mechanisms: bubble collisions, sound waves, and turbulence. Sound waves are often dominant for thermal FOPTs [9–11], but precise modelling involves costly scalar+fluid lattice simulations [12–14]. These simulations rely on adjustable parameters, such as bubble wall velocity v_w, and simplified equations of state (EoS), which introduce uncertainties [15–18].

To improve efficiency, methods such as hybrid simulations and sound shell models [15, 19, 20] have been proposed. However, these rely on simplified EoS and manually set v_w, which can lead to deviations in the GW spectra. Recent studies suggest that sound wave spectra might exhibit double broken-power laws and more intricate features [21].

This work introduces a deterministic framework for PTGW computation which is applicable to any particle physics model. Starting with a Lagrangian that encapsulates the particle physics of a given model, the effective potential V_{eff} is derived to calculate the EoS and nucleation rate Γ. Solving the equations of motion (EoM) for the scalar field and fluid determines v_w and pre-collision hydrodynamics. By generalising hybrid simulations, our method handles realistic EoS and post-collision hydrodynamics. Finally, combining nucleation history and hydrodynamics yields the GW spectrum. We demonstrate this approach with deterministic GW spectra for the SM+$|H|^6$ model. More details of the methodology can be found in references [22, 23].

2. Effective Potential

We consider the SM+$|H|^6$ model, where a dimension-6 operator $|H|^6$ is added to the SM Lagrangian [24–28]. The Higgs potential is given by

$$V(H) = \mu \left(H^\dagger H\right) + \lambda \left(H^\dagger H\right)^2 + \frac{1}{\Lambda^2} \left(H^\dagger H\right)^3 , \tag{1}$$

where Λ is the effective cut-off scale, and μ, λ depend on Λ and SM parameters. This model effectively represents features of new physics extensions like singlet or two-Higgs doublet models [29–32].

The tree-level potential is approximated as

$$V_{\text{eff}}(\phi, T) \approx -\frac{1}{3} a T^4 + \frac{\mu^2 + cT^2}{2} \phi^2 + \frac{\lambda}{4} \phi^4 + \frac{1}{8\Lambda^2} \phi^6, \tag{2}$$

where $a = g_* \pi^2/30$, $g_* \approx 106.75$, and c incorporates gauge and Yukawa couplings [28]. This potential includes the pure $-aT^4/3$ term, crucial for hydrodynamics.

3. Phase Transition Dynamics

The dynamics of a thermal first-order phase transition include bubble wall dynamics and plasma hydrodynamics, described by the equation of state (EoS):

$$p_+(T) = \tfrac{1}{3}aT^4, \quad p_-(T) = \frac{1}{3}aT^4 - \frac{\mu^2 + cT^2}{2}\phi_m^2 - \frac{\lambda}{4}\phi_m^4 - \frac{1}{8\Lambda^2}\phi_m^6, \tag{3}$$

$$e_+(T) = aT^4, \quad e_-(T) = aT^4 + \frac{\mu^2 - cT^2}{2}\phi_m^2 + \frac{\lambda}{4}\phi_m^4 + \frac{1}{8\Lambda^2}\phi_m^6, \tag{4}$$

where $p_\pm$, $e_\pm$ are pressure and energy density in the high/low-temperature phases, and $\phi_m(T)$ is the global minimum of V_{eff}.

The nucleation rate is parameterised as [33, 34]

$$\Gamma(t) \approx \beta_*^4 \exp\left[\beta_*(t - t_*)\right], \tag{5}$$

where $\beta_* = dS_E/dt$ evaluated at $t = t_*$, and t_* is the time corresponding to the reference temperature T_*. The bubble wall velocity, assumed steady-state [35, 36], characterizes wall dynamics and aids in constructing nucleation history. This history is essential for understanding phase transition hydrodynamics.

To determine the steady-state bubble wall velocity v_w, we solve the energy-momentum tensor (EMT) equations for the scalar field and plasma:

$$T^{\mu\nu} = T^{\mu\nu}_\phi + T^{\mu\nu}_{\text{pl}}, \tag{6}$$

where

$$T^{\mu\nu}_\phi = \partial^\mu\phi\partial^\nu\phi - g^{\mu\nu}\left[\frac{1}{2}\partial_\alpha\phi\partial^\alpha\phi - V_0(\phi)\right], \tag{7}$$

$$T^{\mu\nu}_{\text{pl}} = \sum_i \int \frac{d^3\tilde{\mathbf{p}}}{(2\pi)^3 E_{\tilde{p}}}\tilde{p}^\mu\tilde{p}^\nu f_i. \tag{8}$$

Here, $V_0(\phi)$ is the zero temperature potential, and f_i is the particle distribution function. Across the bubble wall, deviations from equilibrium are expressed as $f_i \approx f_i^{\text{eq}} + \delta f_i$, with $f_i^{\text{eq}} = 1/(\exp[\tilde{p}_\mu u^\mu/T] \pm 1)$. The plasma EMT is split into equilibrium and out-of-equilibrium parts:

$$T^{\mu\nu}_{\text{pl}} = T^{\mu\nu}_{\text{eq}} + T^{\mu\nu}_{\text{oeq}}, \tag{9}$$

where $T^{\mu\nu}_{\text{eq}}$ is a perfect fluid and $T^{\mu\nu}_{\text{oeq}}$ includes deviations from equilibrium. The out-of-equilibrium EMT can be written as $T^{\mu\nu}_{\text{oeq}} = T_{\text{oeq,g}}g^{\mu\nu} + T_{\text{oeq},u}$ [36], where

$$\begin{aligned} T_{\text{oeq,g}} =& \frac{1}{2}\sum_i (m_i^2\Delta^i_{00} + \Delta^i_{02} - \Delta^i_{20})\,, \\ T_{\text{oeq},u} =& \frac{1}{2}\sum_i \left[(3\Delta^i_{20} - \Delta^i_{02} - m_i^2\Delta^i_{00})u^\mu u^\nu + (3\Delta^i_{02} - \Delta^i_{20} + m_i^2\Delta^i_{00})\bar{u}^\mu\bar{u}^\nu + 2\Delta^i_{11}(u^\mu\bar{u}^\nu + \bar{u}^\mu u^\nu)\right]. \end{aligned} \tag{10}$$

	Λ [GeV]	T_n [GeV]	β_n/H_n	v_w	$L_w T_n$
BP$_1$	740	95.58	17217	0.43	10.40
BP$_2$	640	73.50	1806	0.99995	4.32

Table 1: Phase transition parameters for our two benchmark points of the SM+$|H|^6$.

The total EMT conservation $\partial_\mu T^{\mu\nu} = 0$ leads to the equations of motion:

$$\partial_z^2 \phi + \frac{\partial V_{\rm eff}}{\partial \phi} + \sum_i \frac{\partial (m_i^2)}{\partial \phi} \frac{\Delta_{00}^i}{2} = 0, \tag{11a}$$

$$\partial_z [w\gamma^2 v + T_{\rm oeq}^{30}] = 0, \tag{11b}$$

$$\partial_z \left[\frac{1}{2}(\partial_z \phi)^2 - V_{\rm eff} + w\gamma^2 v^2 + T_{\rm oeq}^{33} \right] = 0. \tag{11c}$$

The Boltzmann equation governs δf_i and Δ_{mn}^i:

$$\left[\tilde{p}z\partial_z - \frac{1}{2}\partial_z (m_i^2) \partial \tilde{p}_z \right] \delta f_i = C^{\rm lin} + \mathcal{S}_i, \tag{12}$$

where $\mathcal{S}_i$ is derived from equilibrium distributions, and $C^{\rm lin}$ includes scattering processes such as $\bar{t}t \to gg$ and $tg \to tg$ [36–38]. Solving these equations with the Chebyshev spectral method [39] provides v_w.

To determine v_w, boundary conditions for eqs.(11a)-(11c) must be applied, based on the single-bubble hydrodynamics governed by the EoS (10). Integrating eqs.(11a)-(11c) across the wall gives the matching conditions [40, 41]:

$$\begin{aligned} w_+\gamma_+^2 v_+ &= w_-\gamma_-^2 v_-, \\ w_+\gamma_+^2 v_+^2 + p_+ &= w_-\gamma_-^2 v_-^2 + p_-. \end{aligned} \tag{13}$$

The SM+$|H|^6$ model supports detonations ($v_w = |v_+|$), deflagrations ($v_w = |v_-|$), and hybrid modes ($v_- = c_{s,-}$) [22]. The detonation boundary conditions follow directly from eq.(13), while deflagration and hybrid modes require solving fluid profiles between the bubble wall and the shock front using $\partial_\mu T_{\rm eq}^{\mu\nu} = 0$.

For spherical bubbles at steady state, the fluid equations are:

$$\begin{aligned} 2\frac{v}{\xi} &= \gamma^2(1 - v\xi) \left[\frac{\mu^2}{c_s^2(T)} - 1 \right] \partial_\xi v, \\ \partial_\xi T &= T\gamma^2 \mu \partial_\xi v, \end{aligned} \tag{14}$$

where $\mu(\xi, v) \equiv (\xi - v)/(1 - \xi v)$, $\xi \equiv r/t$, and $c_s^2(T) = (dp/dT)/(de/dT)$. At the shock front, eqs.(13) determine its position. The shooting method provides boundary conditions for deflagrations and hybrid modes. Using the profile ansatz $\phi(z) = 0.5\phi_0[1 - \tanh(z/L_w)]$, with $\phi_0 = \phi_m(T_-)$ and L_w the wall width, eqs.(11a)-(11c) are solved iteratively [36] to obtain v_w and fluid profiles. Table 1 summarises v_w, L_w, and other parameters for two benchmark points.

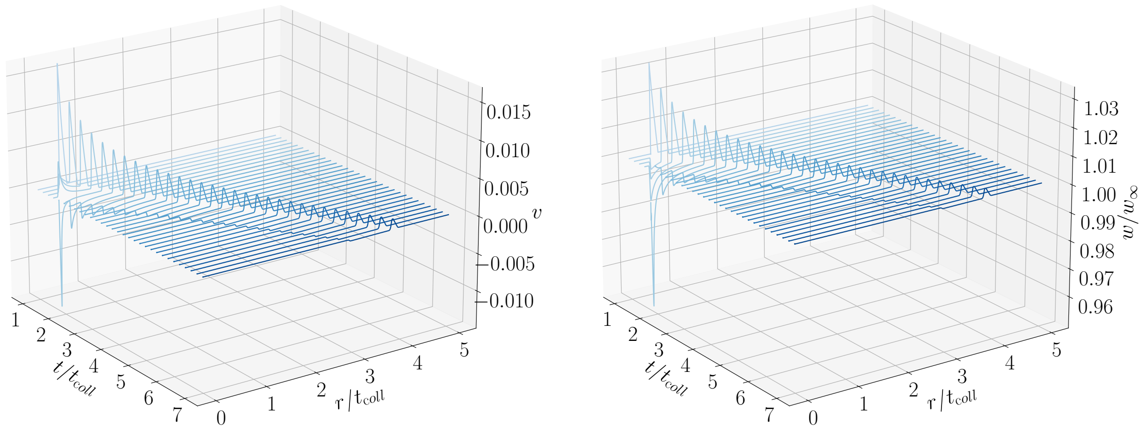

Figure 1: Post-collision fluid profiles for BP_1. **Left**: velocity. **Right**: enthalpy.

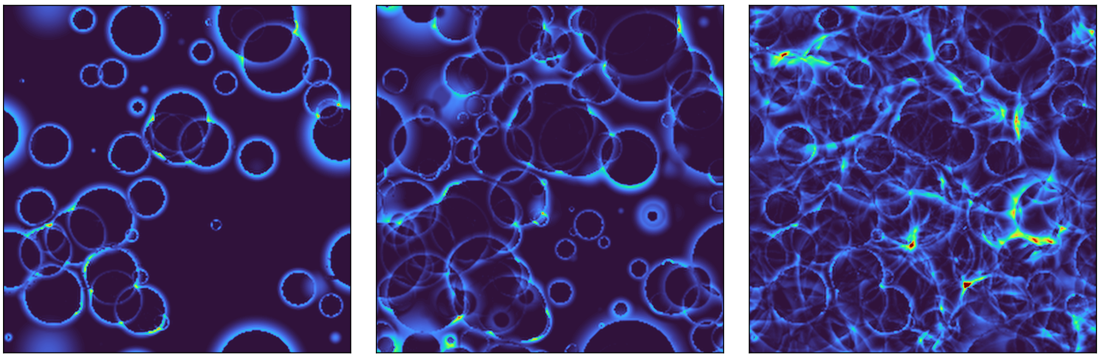

Figure 2: Snapshots of kinetic energy density evolution for BP_1.

After bubble collisions, hydrodynamics evolves based on spherical symmetry. The scalar field quickly disappears, shifting the fluid temperature ahead of the shell. Fluid equations become:

$$\begin{aligned} \partial_t E + \partial_r Z &= -\frac{2}{r} Z, \\ \partial_t Z + \partial_r [Zv + p] &= -\frac{2}{r} Zv, \end{aligned} \tag{15}$$

where $Z \equiv w\gamma^2 v$ and $E \equiv w\gamma^2 - p$. The Kurganov-Tadmor scheme [42] evolves these equations, deriving T from E and Z, and v from Z. Fig. 1 shows fluid profiles for BP_1.

To calculate gravitational waves, the nucleation history combines individual bubbles. Assuming perturbative behaviour [15, 22], hydrodynamic quantities are superimposed:

$$\begin{aligned} \frac{\Delta w}{w_0}(t, \vec{x}) &\simeq \sum_{i:\text{bubbles}} \frac{\Delta w_{\vec{n}i}}{w_0}(t, |\vec{x} - \vec{n}i|), \\ \vec{v}(t, \vec{x}) &\simeq \sum_{i:\text{bubbles}} \vec{v}\vec{n}_i(t, |\vec{x} - \vec{n}_i|). \end{aligned} \tag{16}$$

Snapshots of the evolution of the energy density are shown in Fig. 2.

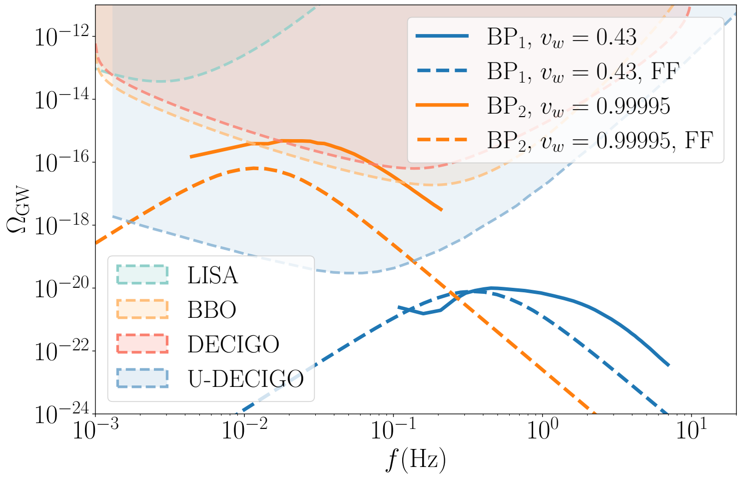

Figure 3: GW spectra for benchmarks in Table 1. Solid lines show results from our scheme; dashed lines use fitting formulae. Shaded regions represent detector sensitivities [44, 45].

3.1 Gravitational Wave Production

Gravitational waves are tensor perturbations h_{ij} of the Friedmann-Robertson-Walker metric, sourced by $T^{\mu\nu}$ through the linearised Einstein equation, $\Box h_{ij} = 16\pi G \Lambda_{ij,kl} T^{kl}$, where G is the Newtonian constant. Assuming a short source duration, the GW spectrum at production time is

$$\Omega^*_{\rm GW}(q) \equiv \frac{1}{\rho_{\rm crit}} \frac{d\rho_{\rm GW}}{d\ln k} \approx \frac{4H^2\tau_{\rm sw}}{3\pi^2\beta} \frac{q^3\beta}{w_\infty^2 \mathcal{V}\mathcal{T}} \int \frac{d\Omega_k}{4\pi} \left[\Lambda_{ij,kl} T_{ij}(q,\vec{k}) T^*_{kl}(q,\vec{k})\right]_{q=|\vec{k}|}, \tag{17}$$

where q is the angular frequency, T_{ij} is the energy-momentum tensor, and $\mathcal{V}, \mathcal{T}$ are simulation volume and time. The lifetime of sound waves is estimated to be $\tau_{\rm sw} \approx R_*/\sqrt{K_{\rm fl}}$, where $K_{\rm fl}$ is the kinetic energy fraction [43], and R_* is the mean bubble separation.

For sound waves, $T^{ij}(t, \vec{x}) = w\gamma^2 v^i v^j$ is constructed from enthalpy and velocity fields (16). Using the projected T^{ij}, the GW spectrum at production is obtained from eq. (17), and redshifting gives the present spectrum:

$$\Omega_{\rm GW}(f) = 3.57 \times 10^{-5} \left(\frac{100}{g_*}\right)^{1/3} \Omega^*_{\rm GW}(q). \tag{18}$$

The frequencies are redshifted as $f(q) \propto q$, where H_* is the Hubble parameter at T_*.

Figure 3 shows the GW spectra for benchmark points. For BP$_1$, the spectrum is below the sensitivity of future detectors. For BP$_2$, the spectrum is within the sensitivity of BBO, DECIGO, and Ultimate-DECIGO but outside the range of LISA's due to higher phase transition strength. Comparison with fitting formulae shows discrepancies in amplitude and shape, particularly for BP$_2$, where our method predicts more complex low-frequency features and a higher amplitude.

The dominant GW source remains sound waves, even for BP$_2$ with ultra-relativistic v_w. The wall energy fraction is $K_{\rm wall} \sim 10^{-10}$, compared to $K_{\rm fl} \sim 10^{-4}$, demonstrating the negligible contribution of the bubble wall to the GW signal. Limitations in computational resources restrict our results to a specific frequency range, with unphysical rises outside this range indicating the bounds of validity.

4. Conclusions

We have developed a self-consistent framework for calculating GWs from FOPTs, addressing key limitations of traditional approaches. Future work will extend this methodology to include refined effective potentials and additional BSM models, paving the way for robust GW predictions in the era of space-based observatories.

Precise PTGW calculations are essential for probing new physics with future space-based GW experiments. Conventional methods suffer from inconsistencies, including the reliance on fitting formulae with incompatible assumptions, simplified EoS treatments, and undetermined bubble wall velocities.

To address these issues, we propose a framework based on hydrodynamic simulation for consistent PTGW calculations in the SM+$|H|^6$. Our approach directly uses the Lagrangian, avoiding approximations. Compared to conventional methods, our results differ significantly in spectral shape and amplitude. Future work could include refined effective potential calculations [46–50] based on dimensional reduction [51, 52], enabling more robust PTGW predictions.

Acknowledgments

We thank Benoit Laurent, Henrique Rubira, Michael Bardsley, and Lachlan Morris for insightful and useful discussions. C.T. is supported by the National Natural Science Foundation of China (Grants No. 12405048) and the Natural Science Foundation of Anhui Province (Grants No. 2308085QA34). X.W. and C.B. are supported by Australian Research Council grants DP210101636, DP220100643 and LE21010001.

References

[1] LIGO Scientific, Virgo collaboration, *Observation of Gravitational Waves from a Binary Black Hole Merger*, *Phys. Rev. Lett.* **116** (2016) 061102 [1602.03837].

[2] NANOGrav collaboration, *The NANOGrav 15 yr Data Set: Evidence for a Gravitational-wave Background*, *Astrophys. J. Lett.* **951** (2023) L8 [2306.16213].

[3] H. Xu et al., *Searching for the Nano-Hertz Stochastic Gravitational Wave Background with the Chinese Pulsar Timing Array Data Release I*, *Res. Astron. Astrophys.* **23** (2023) 075024 [2306.16216].

[4] EPTA, InPTA: collaboration, *The second data release from the European Pulsar Timing Array - III. Search for gravitational wave signals*, *Astron. Astrophys.* **678** (2023) A50 [2306.16214].

[5] D.J. Reardon et al., *Search for an Isotropic Gravitational-wave Background with the Parkes Pulsar Timing Array*, *Astrophys. J. Lett.* **951** (2023) L6 [2306.16215].

[6] LISA collaboration, *Laser Interferometer Space Antenna*, 1702.00786.

[7] W.-R. Hu and Y.-L. Wu, *The Taiji Program in Space for gravitational wave physics and the nature of gravity*, *Natl. Sci. Rev.* **4** (2017) 685.

[8] S. Kawamura et al., *The Japanese space gravitational wave antenna: DECIGO*, *Class. Quant. Grav.* **28** (2011) 094011.

[9] C. Caprini et al., *Science with the space-based interferometer eLISA. II: Gravitational waves from cosmological phase transitions*, *JCAP* **04** (2016) 001 [1512.06239].

[10] C. Caprini et al., *Detecting gravitational waves from cosmological phase transitions with LISA: an update*, *JCAP* **03** (2020) 024 [1910.13125].

[11] P. Athron, C. Balázs, A. Fowlie, L. Morris and L. Wu, *Cosmological phase transitions: From perturbative particle physics to gravitational waves*, *Prog. Part. Nucl. Phys.* **135** (2024) 104094 [2305.02357].

[12] M. Hindmarsh, S.J. Huber, K. Rummukainen and D.J. Weir, *Gravitational waves from the sound of a first order phase transition*, *Phys. Rev. Lett.* **112** (2014) 041301 [1304.2433].

[13] M. Hindmarsh, S.J. Huber, K. Rummukainen and D.J. Weir, *Numerical simulations of acoustically generated gravitational waves at a first order phase transition*, *Phys. Rev. D* **92** (2015) 123009 [1504.03291].

[14] M. Hindmarsh, S.J. Huber, K. Rummukainen and D.J. Weir, *Shape of the acoustic gravitational wave power spectrum from a first order phase transition*, *Phys. Rev. D* **96** (2017) 103520 [1704.05871].

[15] R. Jinno, T. Konstandin and H. Rubira, *A hybrid simulation of gravitational wave production in first-order phase transitions*, *JCAP* **04** (2021) 014 [2010.00971].

[16] R. Jinno, T. Konstandin, H. Rubira and I. Stomberg, *Higgsless simulations of cosmological phase transitions and gravitational waves*, *JCAP* **02** (2023) 011 [2209.04369].

[17] M. Hindmarsh, *Sound shell model for acoustic gravitational wave production at a first-order phase transition in the early Universe*, *Phys. Rev. Lett.* **120** (2018) 071301 [1608.04735].

[18] R. Sharma, J. Dahl, A. Brandenburg and M. Hindmarsh, *Shallow relic gravitational wave spectrum with acoustic peak*, *JCAP* **12** (2023) 042 [2308.12916].

[19] M. Hindmarsh and M. Hijazi, *Gravitational waves from first order cosmological phase transitions in the Sound Shell Model*, *JCAP* **12** (2019) 062 [1909.10040].

[20] A. Roper Pol, S. Procacci and C. Caprini, *Characterization of the gravitational wave spectrum from sound waves within the sound shell model*, *Phys. Rev. D* **109** (2024) 063531 [2308.12943].

[21] L. Giombi, J. Dahl and M. Hindmarsh, *Signatures of the speed of sound on the gravitational wave power spectrum from sound waves*, 2409.01426.

[22] C. Tian, X. Wang and C. Balázs, *Gravitational waves from cosmological first-order phase transitions with precise hydrodynamics*, 2409.14505.

[23] X. Wang, C. Tian and C. Balázs, *Self-consistent prediction of gravitational waves from cosmological phase transitions*, 2409.06599.

[24] X.-m. Zhang, *Operators analysis for Higgs potential and cosmological bound on Higgs mass*, *Phys. Rev. D* **47** (1993) 3065 [hep-ph/9301277].

[25] C. Grojean, G. Servant and J.D. Wells, *First-order electroweak phase transition in the standard model with a low cutoff*, *Phys. Rev. D* **71** (2005) 036001 [hep-ph/0407019].

[26] D.J.H. Chung, A.J. Long and L.-T. Wang, *125 GeV Higgs boson and electroweak phase transition model classes*, *Phys. Rev. D* **87** (2013) 023509 [1209.1819].

[27] F.P. Huang, Y. Wan, D.-G. Wang, Y.-F. Cai and X. Zhang, *Hearing the echoes of electroweak baryogenesis with gravitational wave detectors*, *Phys. Rev. D* **94** (2016) 041702 [1601.01640].

[28] X. Wang, F.P. Huang and X. Zhang, *Phase transition dynamics and gravitational wave spectra of strong first-order phase transition in supercooled universe*, *JCAP* **05** (2020) 045 [2003.08892].

[29] J.R. Espinosa and M. Quiros, *Novel Effects in Electroweak Breaking from a Hidden Sector*, *Phys. Rev. D* **76** (2007) 076004 [hep-ph/0701145].

[30] S. Profumo, M.J. Ramsey-Musolf and G. Shaughnessy, *Singlet Higgs phenomenology and the electroweak phase transition*, *JHEP* **08** (2007) 010 [0705.2425].

[31] C.-W. Chiang, Y.-T. Li and E. Senaha, *Revisiting electroweak phase transition in the standard model with a real singlet scalar*, *Phys. Lett. B* **789** (2019) 154 [1808.01098].

[32] P. Athron, C. Balazs, A. Fowlie, L. Morris, G. White and Y. Zhang, *How arbitrary are perturbative calculations of the electroweak phase transition?*, *JHEP* **01** (2023) 050 [2208.01319].

[33] K. Enqvist, J. Ignatius, K. Kajantie and K. Rummukainen, *Nucleation and bubble growth in a first order cosmological electroweak phase transition*, *Phys. Rev. D* **45** (1992) 3415.

[34] R. Jinno, T. Konstandin, H. Rubira and J. van de Vis, *Effect of density fluctuations on gravitational wave production in first-order phase transitions*, *JCAP* **12** (2021) 019 [2108.11947].

[35] G.D. Moore and T. Prokopec, *Bubble wall velocity in a first order electroweak phase transition*, *Phys. Rev. Lett.* **75** (1995) 777 [hep-ph/9503296].

[36] B. Laurent and J.M. Cline, *First principles determination of bubble wall velocity*, *Phys. Rev. D* **106** (2022) 023501 [2204.13120].

[37] G.D. Moore and T. Prokopec, *How fast can the wall move? A Study of the electroweak phase transition dynamics*, *Phys. Rev. D* **52** (1995) 7182 [hep-ph/9506475].

[38] S. Jiang, F.P. Huang and X. Wang, *Bubble wall velocity during electroweak phase transition in the inert doublet model*, *Phys. Rev. D* **107** (2023) 095005 [2211.13142].

[39] J. Boyd, *Chebyshev and Fourier Spectral Methods: Second Revised Edition*, Dover Books on Mathematics, Dover Publications (2013).

[40] J.R. Espinosa, T. Konstandin, J.M. No and G. Servant, *Energy Budget of Cosmological First-order Phase Transitions*, *JCAP* **06** (2010) 028 [1004.4187].

[41] X. Wang, F.P. Huang and X. Zhang, *Energy budget and the gravitational wave spectra beyond the bag model*, *Phys. Rev. D* **103** (2021) 103520 [2010.13770].

[42] A. Kurganov and E. Tadmor, *New High-Resolution Central Schemes for Nonlinear Conservation Laws and Convection–Diffusion Equations*, *J. Comput. Phys.* **160** (2000) 241.

[43] X. Wang, C. Tian and F.P. Huang, *Model-dependent analysis method for energy budget of the cosmological first-order phase transition*, *JCAP* **07** (2023) 006 [2301.12328].

[44] E. Thrane and J.D. Romano, *Sensitivity curves for searches for gravitational-wave backgrounds*, *Phys. Rev. D* **88** (2013) 124032 [1310.5300].

[45] K. Schmitz, *New Sensitivity Curves for Gravitational-Wave Signals from Cosmological Phase Transitions*, *JHEP* **01** (2021) 097 [2002.04615].

[46] D. Croon, O. Gould, P. Schicho, T.V.I. Tenkanen and G. White, *Theoretical uncertainties for cosmological first-order phase transitions*, *JHEP* **04** (2021) 055 [2009.10080].

[47] P. Schicho, T.V.I. Tenkanen and G. White, *Combining thermal resummation and gauge invariance for electroweak phase transition*, *JHEP* **11** (2022) 047 [2203.04284].

[48] O. Gould and T.V.I. Tenkanen, *Perturbative effective field theory expansions for cosmological phase transitions*, *JHEP* **01** (2024) 048 [2309.01672].

[49] A. Ekstedt, P. Schicho and T.V.I. Tenkanen, *Cosmological phase transitions at three loops: the final verdict on perturbation theory*, 2405.18349.

[50] M. Chala, J.C. Criado, L. Gil and J.L. Miras, *Higher-order corrections to phase-transition parameters in dimensional reduction*, 2406.02667.

[51] K. Farakos, K. Kajantie, K. Rummukainen and M.E. Shaposhnikov, *3-D physics and the electroweak phase transition: Perturbation theory*, *Nucl. Phys. B* **425** (1994) 67 [hep-ph/9404201].

[52] K. Kajantie, M. Laine, K. Rummukainen and M.E. Shaposhnikov, *Generic rules for high temperature dimensional reduction and their application to the standard model*, *Nucl. Phys. B* **458** (1996) 90 [hep-ph/9508379].